HHS Public Access

Author manuscript

Photochem Photobiol Sci. Author manuscript; available in PMC 2020 February 13.

Published in final edited form as:

Photochem Photobiol Sci. 2019 February 13; 18(2): 505–515. doi:10.1039/c8pp00452h.

Sodium Nitrite Potentiates Antimicrobial Photodynamic Inactivation: Possible Involvement of Peroxynitrate.

Ying-Ying Huang[1,2], **Paweł J. Rajda**[3], **Grzegorz Szewczyk**[4], **Brijesh Bhayana**[1], **Long Y Chiang**[5], **Tadeusz Sarna**[4], and **Michael R Hamblin**[1,2,6,*]

[1]Wellman Center for Photomedicine, Massachusetts General Hospital, Boston, MA 02114, USA [2]Department of Dermatology, Harvard Medical School, Boston, MA 02115, USA [3]Faculty of Computer Science, Electronics and Telecommunications, AGH University of Science and Technology, Krakow, Poland [4]Department of Biophysics, Faculty of Biochemistry, Biophysics and Biotechnology, Jagiellonian University, Krakow, Poland [5]Department of Chemistry, University of Massachusetts Lowell, Lowell, MA 01854, USA [6]Harvard-MIT Division of Health Sciences and Technology, Cambridge, MA 02139, USA

Abstract

We have recently shown that a wide range of different inorganic salts can potentiate antimicrobial photodynamic inactivation (aPDI) and TiO_2-mediated antimicrobial photocatalysis. Potentiation has been shown with azide, bromide, thiocyanate, selenocyanate, and most strongly, with iodide. Here we show that sodium nitrite can also potentiate broad-spectrum aPDI killing of Gram-positive MRSA and Gram-negative *Escherichia coli* bacteria. Literature reports have previously shown that two photosensitizers (PS), methylene blue (MB) and riboflavin, when excited by broad-band light in the presence of nitrite could lead to tyrosine nitration. Addition of up to 100 mM nitrite gave 6 logs of extra killing in the case of Rose Bengal excited by green light against *E. coli*, and 2 logs of extra killing against MRSA (eradication in both cases). Comparable results were obtained for other PS (TPPS4 + blue light and MB + red light). Some bacterial killing was obtained when bacteria were added after light using a functionalized fullerene (LC15) + nitrite + blue light, and tyrosine ester amide was nitrated using both “in” and “after” modes with all four PS. The mechanism could involve formation of peroxynitrate by a reaction between superoxide radicals and nitrogen dioxide radicals; formation of the latter species was demonstrated by spin trapping with nitromethane.

*Correspondence: Hamblin@helix.mgh.harvard.edu.

Conflicts of Interest

M. R. Hamblin is on the Scientific Advisory Boards of the following companies: Transdermal Cap Inc, Cleveland, OH; Photothera Inc, Carlsbad, CA; BeWell Global Inc, Wan Chai, Hong Kong; Hologenix Inc. Santa Monica, CA; LumiThera Inc, Poulsbo, WA; Vielight, Toronto, Canada; Bright Photomedicine, Sao Paulo, Brazil; Quantum Dynamics LLC, Cambridge, MA; Global Photon Inc, Bee Cave, TX, Medical Coherence, Boston MA; NeuroThera, Newark DE; JOOVV Inc, Minneapolis-St. Paul MN; Illumiheal & Petthera, Shoreline, WA; MB Lasertherapy, Houston, TX and has consulted for: USHIO Corp, Japan; Merck KGaA, Darmstadt, Germany; Philips Electronics Nederland B.V.; Johnson & Johnson Inc, Philadelphia, PA; UVLRx Therapeutics, Oldsmar, FL; Ultralux UV Inc, Lansing MI; AIRx Medical, Pleasanton CA; FIR Industries, Inc. Ramsey, NJ

Keywords

antimicrobial photodynamic inactivation; sodium nitrite; inorganic salt potentiation; peroxynitrate

Introduction

Antimicrobial photodynamic inactivation (aPDI) is a new approach to killing pathogenic microorganisms, that has taken off in response to growing concerns about the unstoppable spread of multi-drug resistance (MDR). The O'Neill report forecast that if nothing were done to stop it, MDR infections could cost the world 10 million extra deaths and cost $100 trillion by 2050 (1). New approaches are urgently needed, which should not themselves cause the development of resistance, and should also be effective against MDR pathogens (2). aPDI employs non-toxic photosensitizers (PS) that can be excited with harmless visible light to produce a long-lived triplet state (3). The PS triplet can interact with surrounding oxygen in two different ways. The Type 1 photochemical mechanism involves electron transfer to produce superoxide, hydrogen peroxide and hydroxyl radicals. The Type 2 mechanism involves energy transfer to produce singlet oxygen. The balance between these two pathways depends on the PS structure, the availability of electron donors, and on the concentration of oxygen (4). Both of these groups of reactive oxygen species (ROS) can damage biomolecules (lipids, proteins and nucleic acids) and lead to cell death. Selectivity for microorganisms over surrounding mammalian host cells depends on designing the PS structure to bind and penetrate bacteria (cationic charge), topical application of the PS into the infected area, and on using a short drug-light interval because PS uptake into mammalian cells is relatively slow (5).

We have recently reported that a surprisingly wide range of inorganic salts can potentiate aPDI by a large amount (many orders of magnitude) (6). This phenomenon has been reported with potassium iodide (7–9), potassium bromide (10), potassium thiocyanate (11), potassium selenocyanate (12) and sodium azide (13). The mechanisms of action of these different salts are quite different, and to some extent depend on whether the aPDI process is mainly Type 1 or Type 2. We originally discovered this phenomenon by observing the "paradoxical potentiation of methylene blue-mediated aPDI by sodium azide" (13). Paradoxical because azide is frequently used as a quencher of singlet oxygen, and would be expected to inhibit aPDI. In reality azide does inhibit aPDI where Type 2 mechanisms dominate (14), but for those PS where Type 1 mechanisms are significant (phenothiazinium dyes (15) and fullerenes (16)), azide can actually potentiate aPDI.

There have been several reports from the laboratory of Laura Pecci in Italy, that nitrite could carry out interesting reactions when treated with PDT mediated by different types of PS. These reactions were largely concerned with nitration of tyrosine to produce 3-nitrotyrosine by light-activated MB in the presence of nitrite (17). A similar result was obtained from light-activated riboflavin in the presence of nitrite and tyrosine (18).

Therefore, the goal of the present study was to test whether nitrite could potentiate aPDI, and if so, by what mechanism?

Materials and Method

Chemicals and Materials

All chemicals were used as received without any further purification. Sodium nitrite ($NaNO_2$), potassium iodide (KI), methylene blue (MB), Rose Bengal (RB) and meso-tetra-(4-sulfonatophenyl)-porphine (TPPS4) and all other reagents were purchased from Sigma-Aldrich (St. Louis, MO) unless otherwise indicated. Brain-heart infusion (BHI) was purchased from Fisher Scientific. Amplex® red hydrogen peroxide/peroxidase assay kit (A22188; Molecular Probes) was purchased from Invitrogen (Carlsbad, CA, USA). Nitrite and PS solutions were prepared in dH2O immediately before experiments. LC15 was prepared by Dr. Long Y Chiang (University of Massachusetts Lowell). LC15 was dissolved in dimethylacetamide as a stock solution of 2.5 mM and diluted to 10 μM in PBS immediately before experiment with 10 mins sonication. All the aPDT experiments were carried out using 24-well plates. The structures of the four different PS used are shown in Figure 1.

Microbial strains and culture conditions

The following microbial strains were used in the experiment: *Escherichia coli* (*E. coli*) K12, methicillin-resistant *Staphylococcus aureus* (MRSA US-300). Planktonic *E. coli*, MRSA were cultured in BHI broth in Erlenmeyer flask overnight in incubator-shaker with speed of 150 rpm at 37°C. An aliquot of 1 ml from an overnight suspension was refreshed in fresh BHI (MRSA and *E. coli*) for 2 hours at 37°C to reach mid-log phase. Cell numbers of MRSA and *E. coli* were estimated by measuring the optical density (OD) at 600 nm (OD of 0.6=10^8 cells/ml). The microbial cells suspension was centrifuged, washed, and resuspended in pH7.4 phosphate buffer saline (PBS) to arrest microbial growth and used (10^8 CFU) for the *in vitro* experiments.

Light source

LumaCare™ Lamp Model LC-122 Medical with 660 nm and 540 nm fiber optic probe was used for MB and RB respectively. Emission spectra measurement of this lamp by a spectroradiometer (SPR-01; Luzchem Research Inc. Ottawa, ON, Canada) showed a peak emission at 540 nm for 540 nm fiber optic probe and 660 nm for 660 nm fiber optic probe. Blue light was delivered by an Omnilux Clear-U light-emitting diode (LED) array (Photo Therapeutics, Inc., Carlsbad, CA) with a peak wavelength of 415 nm. The irradiance for all experiments was 50 mW/cm^2 as measured with a power meter (Coherent, Santa Clara, California).

Potentiation of aPDT by addition of sodium nitrite *in vitro*.

A 500 μL cell suspension in PBS consisting of 10^8 cells/mL bacteria were mixed with various concentrations of the PS with or without nitrite in a 24-well plate at room temperature. The 24-well plate was illuminated at room temperature using Lumacare to deliver 0–10 J/cm^2 light. Cells treated with MB, RB or TPPS4 (0–10 μM) and nitrite (0, 100 or 200 mM) in the dark were incubated covered with aluminum foil for the same time as the aPDT groups (15 minutes). At the completion of illumination (or dark incubation), aliquots

(10 μL) were taken from each well to determine colony-forming units (CFUs). The aliquots were serially diluted 10-fold in PBS to give dilutions of 10^{-1} to 10^{-5} times in addition to the original concentration, and 10 μL aliquots of each of the dilutions were dropped on square BHI agar plates. Plates were put in the hood to dry for 15 mins and then incubated for 16–18 hours at 37°C in the dark to allow colony formation. Colonies were counted and colony forming units (CFU) calculated according to (# of colonies × dilution factor)/volume plated=CFU/mL. Survival fractions were routinely expressed as ratios of CFU of microbial cells treated with light and PS/$NaNO_2$ (or PS/$NaNO_2$ in the absence of light) to CFUs of microbes treated with neither. Each experiment was performed at least three times.

Amplex red assay for hydrogen peroxide

Amplex® red hydrogen peroxide/peroxidase assay kit was used to detect the production of H_2O_2 from PS and nitrite mediated PDT in solution. The colorless probe Amplex red (10-acetyl-3, 7-dihydroxy-phenoxazine) reacts with H_2O_2 in the presence of peroxidase and forms resorufin (7-hydroxy-3H-phenoxazin-3-one). The detection process after PS and nitrite mediated PDT was according to manufacturer's instructions. 10 μM of RB, MB or LC15 with addition of 100 mM sodium nitrite were illuminated with increasing fluence of green light, red light or blue light respectively. 50 μL aliquot was withdrawn from each time points and mixed with 50 μl Amplex Red (50 μM) reagent and 0.1 U/mL horseradish peroxidase (HRP) in Krebs–Ringer phosphate (consists of 145 mM NaCl, 5.7 mM Na3PO4, 4.86 mM KCl, 199 0.54 mM CaCl2, 1.22 mM MgSO4, 5.5 mM glucose, pH 7.35). After 30 min incubation, the incremental fluorescence ($\lambda_{ex}/\lambda_{em}$ = 530/590 nm) after an incremental fluence of delivered light was measured by a microplate reader (SPECTRA-max M5, Molecular Devices, USA). Each experiment was repeated three times.

Tyrosine nitration

Sample solutions for the "in format" (total volume 400 μL) contained PS (RB, MB, TPPS4, or LC15 at 10 μM), $NaNO_2$ (100mM) and N-acetyl-L-tyrosine ethyl ester (1 mM) in phosphate buffer (pH 7.4, containing 10% methanol) were irradiated by light (540 nm for RB; 660 nm for MB; 415 nm for TPPS4; 415 nm for LC15) with magnetic stirring. It was necessary to use relatively large fluences of light (100 J/cm^2) in order to get enough product to allow measurement of the peak area. For the "after format" the solution that was illuminated contained PS (RB, MB, TPPS4, or LC15 at 10 μM) plus $NaNO_2$ (100mM). The same light was delivered as before. At the end of the illumination sufficient N-acetyl-L-tyrosine ethyl ester was added to make the final concentration to 1 mM and the solution was immediately mixed and allowed to react for 30 minutes. The LC-MS analyses were performed aliquots of 50 μL of the reaction mixture on an Agilent 1260 LC system equipped with a triple-quad mass spectrometer. The LC conditions were: column: C18, 2.1 × 50 mm, 1.8 μm; elution gradient: solution A = acetonitrile, solution B = 10 mM ammonium acetate in water, 2% −> 100% of A over 6 min with a flow rate of 0.2 mL/min; ionization mode: negative; injection volume: 5 μL. The mass of the molecular ion of N-acetyl-3-nitro-L-tyrosine ethyl ester was 296.

Oxygen photoconsumption measurements

Time-dependent changes in oxygen concentration induced by photoexcitation of rose Bengal were determined by electron paramagnetic resonance (EPR) oximetry using 0.1 mM mHCTPO as dissolved oxygen-sensitive spin probe. Samples containing 25 μM RB in PBS, pH 7.2, were irradiated in EPR quartz flat cells in the resonant cavity with 516–586 nm (35 mW/cm2) light derived from a 300-W high pressure compact arc xenon lamp (Cermax, PE300CE-13FM/Module300W; PerkinElmer Opto-electronics, GmbH, Wiesbaden, Germany) equipped with a water filter, heat reflecting mirror, cut-off filter blocking light below 390 nm and green additive dichroic filter 585FD62–25 (Andover Corporation, Salem, NC, USA). EPR samples were run using microwave power 1.06 mW, modulation amplitude 0.006 mT, scan width 0.3 mT, and scan time 21 s. EPR measurements were carried out using a Bruker EMX-AA EPR spectrometer (Bruker BioSpin, Rheinstetten, Germany).

EPR-spin trapping of nitrogen dioxide

The spin trapping experiments were carried out using the conditions described by Bilski et al. (19). Briefly, $NaN0_2$ was added to 1 ml of a 0.5 M NaOH solution containing 0.1 mM RB to give about 1 mM $NaNO_2$ concentration, at pH ~13.5. To the 1 ml solution, either in equilibrium with air or deaerated by bublling with argon, a drop of nitromethane was added, giving about 0.1 M nitromethane. The complete solution was then drawn into a quartz flat cells, which was inserted into a resonant cavity and irradiated with green light as described in section above.

Determination of peroxynitrate in model systems

All samples were prepared in PBS with 0.1 mM diethylenetriaminepentaacetic acid (DTPA). Samples containing Rose Bengal (0.01 mM), sodium nitrite (100 mM) and coumarin boronic acid (CBA, 0.1 mM) were irradiated with green fluorescent COB LED (520–580 nm, 10 mW/cm2) for 5 minutes. In control samples, H_2O_2 (0.05 mM) and/or catalase (250 units/mL) were added to check for possible oxidation of CBA by hydrogen peroxide. Some samples were oxygen depleted by saturating with argon for 10 minutes. Fluorescence intensity of formed COH in samples was measured by a plate reader (ClarioStar, BMG Labtech, USA), (360 nm excitation/465 nm emission) for 11 minutes.

Direct detection of singlet oxygen

Time-resolved singlet oxygen generation and quenching was carried out as follows.

Phosphate-buffered (pH 7.2) D_2O solution of RB (optical density ~0.25–0.3 at 550 nm) in a 1-cm-optical path quartz fluorescence cuvette (QA-1000; Hellma, Mullheim, Germany), was excited with 550 nm pulses generated by an integrated nanosecond DSS Nd:YAG laser system equipped with a narrow bandwidth optical parametric oscillator (NT242–1k-SH/SFG; Ekspla, Vilnius, Lithuania), which delivered pulses at repetition rate 1 kHz, with energy up to several hundred microjoules in the visible region. Due to high efficiency of singlet oxygen photogeneration by RB, the energy of the exciting pulses was attenuated ~400 times. The near-infrared luminescence (1270 nm) was measured perpendicularly to the excitation beam in a photon-counting mode using a thermoelectric cooled NIR PMT module (H10330–45; Hamamatsu, Japan) equipped with a 1100-nm cutoff filter and an additional

dichroic narrow-band filter NBP, selectable from the spectral range 1150–1355 nm (NDC Infrared Engineering Ltd, Bates Road, Maldon, Essex, UK). Data were collected using a computer-mounted PCI-board multichannel scaler (NanoHarp 250; PicoQuant GmbH, Berlin, Germany). Data analysis, including first-order luminescence decay fitted by the Levenberg–Marquardt algorithm, was performed by custom-written software. Typical acquisition time was 20 s. The effect of nitrite on singlet oxygen lifetime was examined in the concentration range 0 to 200 mM.

Laser flash photolysis measurements

To control instrumental parameters and facilitate the fast data acquisition in laser flash photolysis experiments, a dedicated system has been designed and built. The unit includes a programmable HV power supply for PMT, a fast (flash) 14-bit 400 MS/ps A/D Converter for PMT signal acquisition and several slow-control ADCs and DACs. The heart of the unit is based on a All-Programmable Xilinx Zynq device, which contains ARM A9 microcontroller (with peripheral interfaces: SPI, ETH, UART, GPIO) and some programmable logic resources, which have been utilized for the implementation of time-critical functions, such as PMT signal reception / storage and precise pulses generation for the laser control. The unit also controls the monitoring beam shutter and monochromator mounted on the PMT. The unit is operated by software developed with LabVIEW environment and runs by a designated PC.

Results

Nitrite potentiates aPDI.

We first tested the addition of sodium nitrite (100 mM) to aPDI with RB activated by 540 nm light. It had become clear with our other studies using other inorganic salts to potentiate aPDI, that relatively high concentrations of salt (at least 100 mM) were necessary to obtain the maximum effect. RB is known to be very efficient at mediating aPDI against Gram-positive bacteria like MRSA (good activity at concentrations < 1 μM), but almost completely inactive against Gram-negative *E. coli* (20). In Figure 2A we see that addition of nitrite gives 2–3 logs more killing compared to the killing seen with RB-aPDI alone. In Figure 2B we see that the results against *E. coli* were even more impressive. There was essentially zero killing using RB-aPDI alone, while when nitrite was added, we obtained eradication (> 6 logs of killing) with RB concentrations of 5 μM and 10 μM. The analogous results with porphyrin TPPS4 activated by 415 nm light are shown in Figures 2C and 2D. Against MRSA (Figure 2C) there was more than 2 logs extra killing at a concentration of 50 nM TPPS4 in the presence of 100 mM nitrite, but the differences disappeared at higher concentrations because TPPS4 is highly active against MRSA (7). Against *E. coli* (Figure 2D) the results were again very impressive, with eradication being achieved with 5 and 10 μM TPPS4 + 100 mM nitrite, against zero killing without nitrite. In Figure 2E we show the effects of aPDI mediated by the phenothiziunium dye MB activated by red light against MRSA. The degree of potentiation of killing of MRSA by addition of nitrite was higher with MB than either of the other two PS. This is mainly because MB is not nearly as efficient at killing MRSA in aPDI, as can be seen from the fact that it was necessary to use up to 10 μM of MB instead of < 1 μM of RB and TPPS4. So we were able to obtain 6 extra logs of killing by addition of

nitrite (eradication) at 2.5 μM MB. Using a similar argument, the effect of the addition of nitrite was slightly less impressive when MB was used against *E. coli* because the cationic MB does have some effectiveness on its own against Gram-negative bacteria. Figure 2F shows that at 2.5 μM MB there was 6 extra logs of killing (eradication) in the presence of nitrite.

Nitrite potentiation of killing by a fullerene and comparison between "in" and "after" light.

In order to demonstrate the formation of a more or less stable antimicrobial species, and distinguish them from highly reactive species such as radicals and excited states, it is useful to mix the inorganic salt with the PS, deliver the correct amount of light and then immediately add the bacterial cells. However, these antibacterial species although not excited states, may still be unstable or less stable. For instance molecular iodine is stable long term (8), while hypoiodite decays over 1–2 hours (21), and selenocyanogen decays over 20–40 minutes (12). We were not able to show any "after" killing using either bacterial species with any of the PS (RB, TPPS4, or MB) at the concentrations we studied in Figure 3 and with addition of 100 or 200 mM $NaNO_2$ (data not shown). However, this observation does not necessarily mean that stable antibacterial species are not produced, since if they are fairly unstable, the light delivery period (20 minutes) becomes important. If the antibacterial species only has a short half-life (a few minutes) then most of the species that was produced during the illumination would have decayed by the time the bacteria are added.

Therefore, we tested another different PS, the functionalized decacationic fullerene derivative known as LC15 and prepared by Long Y Chiang (16). Figure 3A shows the effect of addition of 100 mM nitrite to aPDI using "in format" with LC15 at increasing concentrations excited by 10 J/cm^2 of blue light against MRSA. While LC15 alone has hardly any activity, needing the highest concentration of LC15 (10 μM) to get any killing at all (< 1 log), the addition of 100 mM nitrite produced eradication at 10 μM, and gave 5 logs of killing at only 5 μM. Figure 3B shows that against *E. coli* there was a very similar and marked degree of potentiation by addition of 100 mM nitrite (eradication at 10 μM). In Figure 3C we show that indeed it was possible to obtain killing in the "after format" using LC15, but we needed to use high concentrations (20 and 50 μM LC15), a higher concentration of 200 mM $NaNO_2$ and high doses of light (20 or 40 J/cm^2 of 415 nm) in order to see any 'after" killing. Even then we were not able to achieve eradication (only 5.5 logs of killing). Again, we found similar results against *E. coli* with "after" killing achieved with the use of high doses of LC15 and light (Figure 3D). After we had gathered these results we went back and tried again with MB + 200 mM nitrite + light in the "after format" against MRSA. We only achieved about 1 log of killing with high doses of MB and light (data not shown). However, even this low degree of "after" killing showed that the phenomenon was general in nature, and did not only apply to the LC15 fullerene.

Mechanistic studies.

The first question we asked was, is the consumption of oxygen increased by irradiating RB in the presence of nitrite. This was carried out by the Sarna laboratory using EPR oximetry as previously described (22). In Figure 4A we see a robust consumption of oxygen occurring in a nitrite-concentration dependent manner when 5 μM RB was excited with green light (35

mW/cm^2). Next we asked if singlet oxygen was being quenched by nitrite? This was carried out by the Sarna laboratory using time-resolved measurement of 1270 nm luminescence emitted from $^1O_2$. Figure 4B shows an inverse linear relationship between the concentration of nitrite and the lifetime of $^1O_2$. The pseudo-first order rate constant of quenching of singlet oxygen by $NaNO_2$ was estimated to be 8.4×10^4 $M^{-1}s^{-1}$.

We next attempted to detect the formation of $NO_2^{\bullet}$ by spin-trapping with nitromethane. In alkaline solutions, nitroalkanes (RCH_2NO_2) undergo deprotonation and rearrangement to form an "aci anion" ($RHC=NO_2-$), which can function as a spin trap (23). The results shown in Fig. 5 clearly demonstrate that nitrogen dioxide is generated upon irradiation of samples containing Rose Bengal and nitrite with green light. The observed 10-line EPR spectrum (Fig 5A) is fully consistent with the dinitromethyl anion radical formed by the interaction of nitrogen dioxide with aci anion of nitromethane, as reported by Pace (24).

It is important to stress that upon irradiation of samples containing RB, nitrite and strongly alkaline solution of nitromethane, the EPR signal develops regardless of the presence of oxygen, which only affects the kinetics of the spin adduct accumulation and its stability (Fig 5B).

Next, we asked whether nitrite could quench the RB triplet state. The goal of this experiment was to answer the question of exactly how the NO_2 was formed.

As can be seen in Figure 6A, addition of 20 mM nitrite to deaerated solution of RB markedly reduced the observable lifetime of the dye triplet excited state monitored at 600 nm. The effect was even stronger in the presence of 100 mM nitrite. Nitrite had also a profound effect on the Rose Bengal radical anion, monitored at 420 nm (Fig 6C); the signal intensity of this species significantly increased with increasing concentration of $NaNO_2$. The quenching rate constant of the RB excited triplet state by nitrite can be obtained by plotting the reciprocal of the triplet lifetime as a function of added nitrite concentration (Fig 6B). The corresponding rate constant is calculated to be 1.9×10^5 $M^{-1}s^{-1}$

The formation of nitrogen dioxide, via one-electron oxidation of nitrite by the excited triplet state of Rose Bengal, as well as the corresponding formation of Rose Bengal radical anion, which is easily reduced by molecular oxygen to superoxide anion (25), raises the intriguing possibility of generation of peroxynitrate, as a product of the interaction of nitrogen dioxide with superoxide anion. Such a reaction between superoxide anion and nitrogen monoxide is well known for it leads to the formation of peroxynitrite and occurs with the rate constant approaching the diffusion limit (26). The reaction between superoxide anion and nitrogen dioxide was studied using pulse radiolysis by Logager and Sehested (27). The authors found that the rate constant of this reaction was rather high (4.5×10^9 $M^{-1}s^{-1}$) and the product was peroxynitrate. Therefore to confirm experimentally that the photosensitized reaction mediated by RB in the presence of nitrite could also lead to the formation of peroxynitrate, we used coumarin boronic acid (CBA), which upon oxidation by appropriate oxidants is converted to fluorescent 7-hydroxycoumarine (COH) (28). Although CBA is oxidized by hydrogen peroxide, the reaction rate constant is 5–6 orders of magnitude lower than that of peroxynitrite. Considering that both peroxynitrite and peroxynitrate have similar two-

electron reduction potentials, it can be expected that peroxynitrate will react with CBA with comparable efficiency to peroxynitrite. Indeed, our data shown in Fig 7 confirm this. Thus, the data indicate that while singlet oxygen is not involved in oxidation of CBA to fluorescent COH, strong oxidation of CBA is observed in irradiated samples containing RB and nitrite. In addition, although H_2O_2 at relatively high concentration is able to oxidize CBA, the effects are much smaller than those induced by photosensitized reaction in the presence of $NaNO_2$. Therefore, the data are consistent with the formation of peroxynitrate via generation of nitrogen dioxide and superoxide anion.

Production of hydrogen peroxide

The Amplex red assay was used to measure the formation of hydrogen peroxide. Figure 8 shows that there was a marked increase in the generation of H_2O_2 by addition of nitrite (100 mM) with all three different PS. Interestingly, the magnitude of the increase appeared to inversely depend on the level of H_2O_2 production without addition of nitrite. The biggest increase (30-fold) was found with RB and green light where the level without nitrite was lowest (875 at 30 J/cm^2). Next with MB and red light there was a 13-fold increase, while the level without nitrite was 1459 at 30 J/cm^2. Finally, with LC15 and blue light there was only a 1.3 fold, increase but the level without nitrite was much higher at 8416. These data suggest that Type 2 photochemistry (singlet oxygen) is leading to the production of H_2O_2 in the presence of nitrite. It should be noted that singlet oxygen often forms hydrogen peroxide when it has carried out a 2-electron oxidation.

Tyrosine nitration.

In order to detect the formation of reactive nitrogen species that could nitrate tyrosine (as reported by Pecci et al (17, 18)) we tested whether illumination (100 J/cm^2) of a mixture of PS (10 μM) with nitrite (100 mM) in the presence of 1 mM N-acetyl-tyrosine ethyl ester, as a model tyrosine substrate suitable for nitration (29) could produce nitration. We tested this reaction in two formats: “in” where all the ingredients were present together during the illumination; and “after” where the light was delivered to a mixture of PS and $NaNO_2$, and then immediately after the light, the N-acetyl-tyrosine ethyl ester was added and mixed. Figure 10 shows the results of the nitrotyrosine formation calculated as area under the curve obtained from the LC-MS chromatograms. In the “in” format the order was MB > RB > TPPS4. LC15 was higher than TPPS4 and equal to RB. In the “after” format the order was similar, except that LC15 was the lowest.

Discussion

Sodium nitrite has now joined the number of different inorganic salts that have been shown to dramatically potentiate aPDI against both Gram-positive and Gram-negative bacteria (6). Azide was the first we reported (13), followed by iodide (9), bromide (10), thiocyanate (11), selenocyanate (12), and finally nitrite. Interestingly, the mechanisms of action appear to be somewhat different in nearly every single case. In the case of azide, the mechanism involves the formation of azide radicals by a 1-electron transfer reaction (13). The mechanism of iodide potentiation involves two pathways, firstly addition of singlet oxygen to iodide to form peroxyiodide which subsequently decomposes to for free iodine, and secondly a 1-

electron transfer to form iodine radicals (8, 9). The mechanism for thiocyanate involves a two-step process to eventually form sulfur trioxide radical anion (11). Selenocyanate involves a two-electron oxidation by singlet oxygen to form selenocyanogen (30, 31).

The ability of nitrite to potentiate some photodynamic effects of different PS has been known since Laura Pecci reported in 2001 (17) that the addition of sodium nitrite to a mixture of tyrosine and methylene blue activated by broad-band white light. led to the formation of 3-nitrotyrosine (3-NT). The fact that the yield of 3-NT was 50% higher in D_2O than in H_2O led them to propose that singlet oxygen was involved in the reaction. Their proposed mechanism was the formation of tyrosine radicals by $^1O_2$ attack on tyrosine. These radicals then reacted with $NO_2^{\bullet}$ radicals that had been produced by one electron oxidation of nitrite. In 2012 the same group reported similar results, this time using riboflavin as the PS (18).

Our data suggest that the antimicrobial species that kills bacteria when nitrite is added into aPDT has a short but measurable lifetime, but not as short lived as $^1O_2$ or $HO^{\bullet}$. Our leading hypothesis is that this species is peroxynitrate, $O_2NO_2^-$. The formation of peroxynitrate from the reaction of superoxide with nitrogen dioxide has been documented by a pulse radiolysis study by Logager and Sehested (32). These authors measured the rate constant to be 4.5exp9 $M^{-1}s^{-1}$. Although the reaction is three fold slower than that of the reaction between superoxide with nitric oxide to form peroxynitrite (26), it is still a very fast reaction, which is bound to occur if NO_2 and superoxide are formed in the same system, at approximately the same time. Based on a theroretical treatment, the similarities and differences between peroxynitrite and peroxynitrate were discussed (33). The main conclusion was that both species have similar barriers for O-atom transfer reaction to heteroatoms and double bonds, which is consistent with the authors' earlier DFT calculations predicting that ONOOH (as well as O2NOOH) should be capable of oxidizing sulfides to sulfoxide and alkenes to epoxides (34). For ONOOH such reactions have been confirmed experimentally (35). The two electron reduction potentials were estimated to be: for peroxynitrite 1.68 V, and for peroxynitrate 1.83 V. Therefore at least thermodynamically, peroxynitrate should be a more potent oxidant than peroxynitrite.

The relative contributions of Type 1 and Type 2 photochemistry to the different observed effects of the addition of nitrite to different PS excited by light is somewhat confusing and contradictory. There were five measured effects in this study all of which were enhanced to greater or lesser degrees by addition of nitrite. (1) Killing of bacteria using "in format"; (2) Killing of bacteria using "after format"; (3) Oxidation of CBA to COH; (4) Production of H_2O_2; (5) Nitration of tyrosine. We used four different PS, LC15, MB, RB and TPPS4. We assumed that these four PS when arranged in the order of most Type 1 and least Type 2 were as follows (Type 1) LC15 > MB > RB > TPPS4 (Type 2). The order of potentiation by nitrite of bacterial killing using the "in" format was TPPS4 ≈ RB > MB > LC15. The order of potentiation by nitrite in bacterial killing in the "after" format was LC15 >> MB with no "after" killing observed using RB and TPPS4. The only PS tested with CBA oxidation was RB, so no comparisons could be made. The order of production of H_2O_2 with addition of nitrite was RB > MB > LC15 (TPPS4 was not tested). The order of nitration of tyrosine was MB > RB ≈ LC15 > TPPS4 using the "in" format, and MB > RB > TPPS4 > LC15 using the

"after" format. Thus, it appears that the species responsible for bacterial killing may be somewhat different from the species that is responsible for tyrosine nitration. Singlet oxygen is most likely to be involved in producing the antibacterial species, while RType I ROS may be more involved in producing the tyrosine nitrating species.

One question worth asking is, how does nitrite compare with the other inorganic salts that we have shown can potentiate aPDI? Iodide is the most versatile and powerful salt because it can work with most PS and at lower concentrations (6). Next most powerful is selenocyanate in terms of versatility and power (30, 31). Nitrite comes next, and the least powerful and versatile are thiocyanate (11), azide (13) and bromide (10).

One of the main attractions of using inorganic salts to potentiate aPDT, is their generally low toxicity. This definitely applies to nitrite. Nitrite has been used in food as a preservative, flavoring agent and color stabilizer for hundreds of years (36). The concentration we used in our present studies is much higher than found in foodstuffs (37), but if nitrite were used medically in a PDT treatment it would be topically applied and not consumed regularly. Nitrite has been used therapeutically as a vasodilator in cardiovascular medicine and various ischemic disorders (38). There has been concern that long-term consumption or exposure to nitrites could be carcinogenic as nitrite can form nitrosamines in the acidic conditions of the stomach (39). However, Butler posed the question "Nitrites and nitrates in the human diet: Carcinogens or beneficial hypotensive agents?" (40) suggesting that the beneficial effects could outweigh any possible harm.

In conclusion, we have shown that the non-toxic inorganic salt, sodium nitrite is able to potentiate the bacterial killing produced by several different PS by up to six logs. The mechanism could possible involve peroxynitrate. In addition to potassium iodide, nitrite is one of the in organic salts most likely to move into clinical applications.

Acknowledgements

This work was supported by US-NIH grants R01AI050875 and R21AI121700. Research carried out at the Jagiellonian University (T.S) was supported by grants from the National Science Centre (2011/03/B/NZ1/00007 and 2013/08/W/NZ3/00700).

References

1. O'Neill J. Tackling a global health crisis:initial steps. The Review on Antimicrobial Resistance Chaired by Jim O'Neill. 2015.
2. Bush K, Courvalin P, Dantas G, Davies J, Eisenstein B, Huovinen P, et al. Tackling antibiotic resistance. Nat Rev Microbiol. 2011;9(12):894–6. [PubMed: 22048738]
3. Castano AP, Demidova TN, Hamblin MR. Mechanisms in photodynamic therapy: part one--photosensitizers, photochemistry and cellular localization. Photodiagnosis Photodyn Ther. 2004;1(4):279–93. [PubMed: 25048432]
4. da Silva Baptista M, Cadet J, Di Mascio P, Ghogare AA, Greer A, Hamblin MR, et al. Type I and II Photosensitized Oxidation Reactions: Guidelines and Mechanistic Pathways. Photochem Photobiol. 2017.
5. Sharma SK, Mroz P, Dai T, Huang YY, St Denis TG, Hamblin MR. Photodynamic Therapy for Cancer and for Infections: What Is the Difference? Isr J Chem. 2012;52(8–9):691–705. [PubMed: 23248387]

6. Hamblin MR. Potentiation of antimicrobial photodynamic inactivation by inorganic salts. Expert Rev Anti Infect Ther. 2017;15(11):1059–69. [PubMed: 29084463]
7. Huang L, El-Hussein A, Xuan W, Hamblin MR. Potentiation by potassium iodide reveals that the anionic porphyrin TPPS4 is a surprisingly effective photosensitizer for antimicrobial photodynamic inactivation. J Photochem Photobiol B. 2017;178:277–86. [PubMed: 29172135]
8. Huang L, Szewczyk G, Sarna T, Hamblin MR. Potassium Iodide Potentiates Broad-Spectrum Antimicrobial Photodynamic Inactivation Using Photofrin. ACS Infect Dis. 2017;3(4):320–8. [PubMed: 28207234]
9. Vecchio D, Gupta A, Huang L, Landi G, Avci P, Rodas A, et al. Bacterial photodynamic inactivation mediated by methylene blue and red light is enhanced by synergistic effect of potassium iodide. Antimicrob Agents Chemother. 2015;59(9):5203–12. [PubMed: 26077247]
10. Wu X, Huang YY, Kushida Y, Bhayana B, Hamblin MR. Broad-spectrum antimicrobial photocatalysis mediated by titanium dioxide and UVA is potentiated by addition of bromide ion via formation of hypobromite. Free Radic Biol Med. 2016;95:74–81. [PubMed: 27012419]
11. St Denis TG, Vecchio D, Zadlo A, Rineh A, Sadasivam M, Avci P, et al. Thiocyanate potentiates antimicrobial photodynamic therapy: In situ generation of the sulfur trioxide radical anion by singlet oxygen. Free Radic Biol Med. 2013;65C:800–10.
12. Huang L, Xuan W, Zadlo A, Kozinska A, Sarna T, Hamblin MR. Antimicrobial photodynamic inactivation is potentiated by addition of selenocyanate: possible involvement of selenocyanogen? J Biophotonics. 2018.
13. Huang L, St Denis TG, Xuan Y, Huang YY, Tanaka M, Zadlo A, et al. Paradoxical potentiation of methylene blue-mediated antimicrobial photodynamic inactivation by sodium azide: role of ambient oxygen and azide radicals. Free Radic Biol Med. 2012;53(11):2062–71. [PubMed: 23044264]
14. Huang L, Xuan Y, Koide Y, Zhiyentayev T, Tanaka M, Hamblin MR. Type I and Type II mechanisms of antimicrobial photodynamic therapy: An in vitro study on gram-negative and gram-positive bacteria. Lasers Surg Med. 2012;44(6):490–9. [PubMed: 22760848]
15. Kasimova KR, Sadasivam M, Landi G, Sarna T, Hamblin MR. Potentiation of photoinactivation of Gram-positive and Gram-negative bacteria mediated by six phenothiazinium dyes by addition of azide ion. Photochem Photobiol Sci. 2014;13(11):1541–8. [PubMed: 25177833]
16. Yin R, Wang M, Huang YY, Landi G, Vecchio D, Chiang LY, et al. Antimicrobial photodynamic inactivation with decacationic functionalized fullerenes: oxygen independent photokilling in presence of azide and new mechanistic insights. Free Radic Biol Med. 2015;79:14–27. [PubMed: 25451642]
17. Pecci L, Montefoschi G, Antonucci A, Costa M, Fontana M, Cavallini D. Formation of nitrotyrosine by methylene blue photosensitized oxidation of tyrosine in the presence of nitrite. Biochem Biophys Res Commun. 2001;289(1):305–9. [PubMed: 11708817]
18. Fontana M, Blarzino C, Pecci L. Formation of 3-nitrotyrosine by riboflavin photosensitized oxidation of tyrosine in the presence of nitrite. Amino Acids. 2012;42(5):1857–65. [PubMed: 21479936]
19. Bilski P, Chignell CF, Szychlinski J, Borkowski A, Oleksy E, Reszka K. Photooxidation of organic and inorganic substrates during UV photolysis of nitrite anion in aqueous solution. J Am Chem Soc. 1992;114:549–56.
20. Wen X, Zhang X, Szewczyk G, El-Hussein A, Huang YY, Sarna T, et al. Potassium Iodide Potentiates Antimicrobial Photodynamic Inactivation Mediated by Rose Bengal in In Vitro and In Vivo Studies. Antimicrob Agents Chemother. 2017;61(7).
21. Huang YY, Choi H, Kushida Y, Bhayana B, Wang Y, Hamblin MR. Broad-Spectrum Antimicrobial Effects of Photocatalysis Using Titanium Dioxide Nanoparticles Are Strongly Potentiated by Addition of Potassium Iodide. Antimicrob Agents Chemother. 2016;60(9):5445–53. [PubMed: 27381399]
22. Szewczyk G, Zadlo A, Sarna M, Ito S, Wakamatsu K, Sarna T. Aerobic photoreactivity of synthetic eumelanins and pheomelanins: generation of singlet oxygen and superoxide anion. Pigment Cell Melanoma Res. 2016;29(6):669–78. [PubMed: 27505632]

23. Reszka KJ, Bilski P, Chignell CF. Spin trapping of nitric oxide by aci anions of nitroalkanes. Nitric Oxide. 2004;10(2):53–9. [PubMed: 15135358]
24. Pace MD. Spin Trapping of Nitrogen Dioxide from Photolysis of Sodium Nitrite, Ammonium Nitrate, Ammonium Dinitramide, and Cyclic Nitramines. J Phys Chem. 1994;98:6251–7.
25. Lambert C, Sarna T, Truscott TG. Rose bengal radicals and their reactivity. J Chem Soc, Faraday Trans. 1990;86:3879–82.
26. Nauser T, Koppenol WH. The Rate Constant of the Reaction of Superoxide with Nitrogen Monoxide: Approaching the Diffusion Limit. J Phys Chem A,. 2002;106:4084–6.
27. Loegager T, Sehested K. Formation and decay of peroxynitric acid: a pulse radiolysis study. J Phys Chem. 1993;97:10047–52.
28. Zielonka J, Sikora A, Hardy M, Joseph J, Dranka BP, Kalyanaraman B. Boronate probes as diagnostic tools for real time monitoring of peroxynitrite and hydroperoxides. Chem Res Toxicol. 2012;25(9):1793–9. [PubMed: 22731669]
29. Ieda N, Nakagawa H, Peng T, Yang D, Suzuki T, Miyata N. Photocontrollable peroxynitrite generator based on N-methyl-N-nitrosoaminophenol for cellular application. J Am Chem Soc. 2012;134(5):2563–8. [PubMed: 22239467]
30. Huang L, Xuan W, Sarna T, Hamblin MR. Comparison of thiocyanate and selenocyanate for potentiation of antimicrobial photodynamic therapy. J Biophotonics. 2018:e201800092. [PubMed: 29885019]
31. Huang L, Xuan W, Zadlo A, Kozinska A, Sarna T, Hamblin MR. Antimicrobial photodynamic inactivation is potentiated by the addition of selenocyanate: Possible involvement of selenocyanogen? J Biophotonics. 2018:e201800029. [PubMed: 29488327]
32. Loegager T, Sehested K. Formation and decay of peroxynitrous acid: a pulse radiolysis study. J Phys Chem. 1993;97:6664–9.
33. Olson LP, Bartberger MD, Houk KN. Peroxynitrate and peroxynitrite: a complete basis set investigation of similarities and differences between these NOx species. J Am Chem Soc. 2003;125(13):3999–4006. [PubMed: 12656637]
34. Houk KN, Condorski KR, Pryor WA. Radical and Concerted Mechanisms in Oxidations of Amines, Sulfides, and Alkenes by Peroxynitrite, Peroxynitrous Acid, and the Peroxynitrite−CO2 Adduct: Density Functional Theory Transition Structures and Energetics. J Am Chem Soc. 1996;118:13002–6.
35. Vayssie S, Elias H. Fast Oxidation of Organic Sulfides by Hydrogen Peroxide by In Situ Generated Peroxynitrous Acid. Angew Chem Int Ed Engl. 1998;37(15):2088–90. [PubMed: 29711056]
36. Dahle HK. Nitrite as a food additive. NIPH Ann. 1979;2(2):17–24. [PubMed: 548837]
37. Matallana Gonzalez MC, Martinez-Tome MJ, Torija Isasa ME. Nitrate and nitrite content in organically cultivated vegetables. Food Addit Contam Part B Surveill. 2010;3(1):19–29. [PubMed: 24785312]
38. Nossaman VE, Nossaman BD, Kadowitz PJ. Nitrates and nitrites in the treatment of ischemic cardiac disease. Cardiol Rev. 2010;18(4):190–7. [PubMed: 20539102]
39. Tenovuo J. The biochemistry of nitrates, nitrites, nitrosamines and other potential carcinogens in human saliva. J Oral Pathol. 1986;15(6):303–7. [PubMed: 3093650]
40. Butler A. Nitrites and nitrates in the human diet: Carcinogens or beneficial hypotensive agents? J Ethnopharmacol. 2015;167:105–7. [PubMed: 25300670]

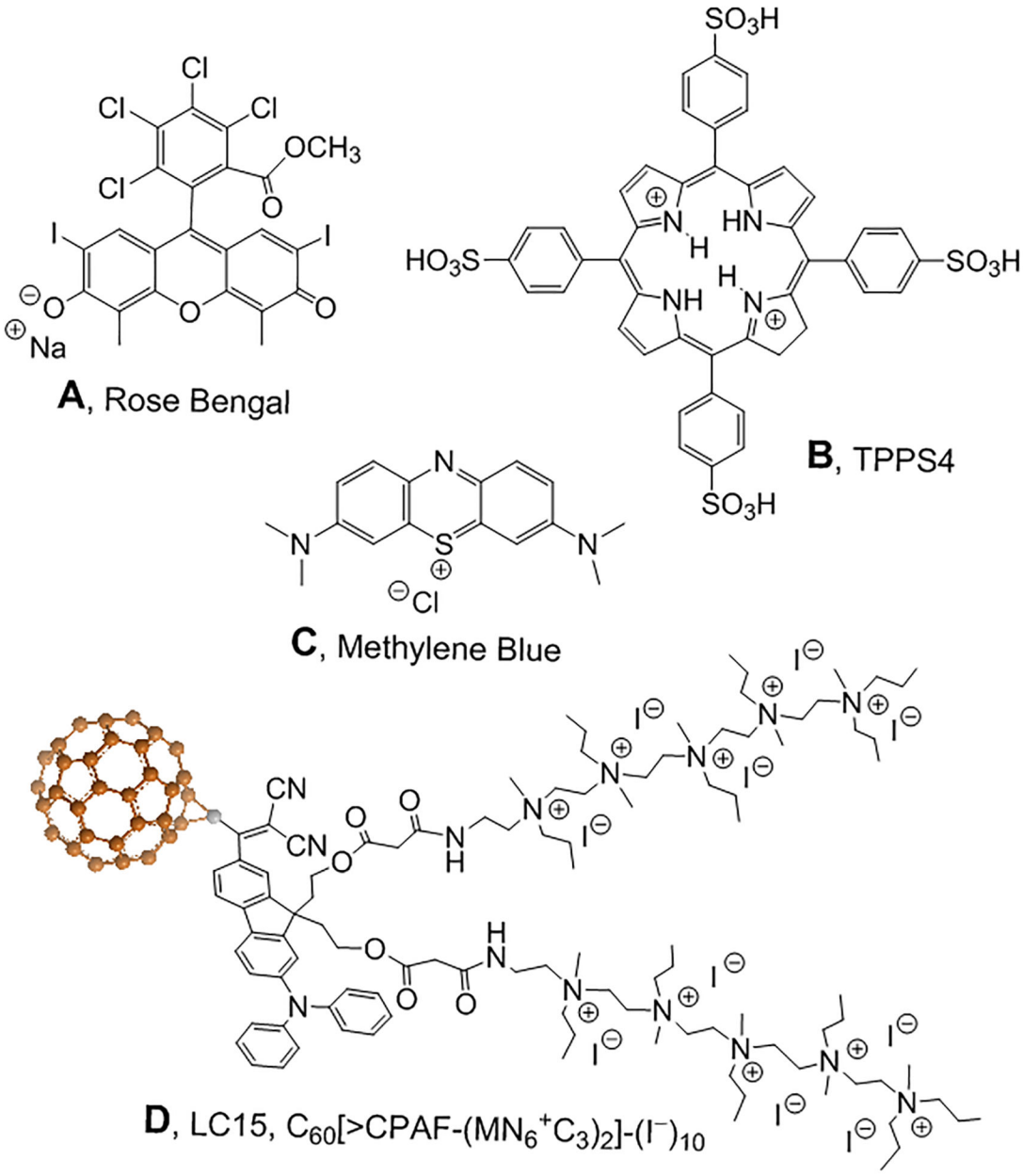

Figure 1. Chemical structures of the four PS.

(A) Rose Bengal, RB; (B) Meso-tetra-(4-sulfonatophenyl)-porphine TPPS4; (C) Methylene blue, MB; (D) Decacationic functionalized fullerene, LC15 (16).

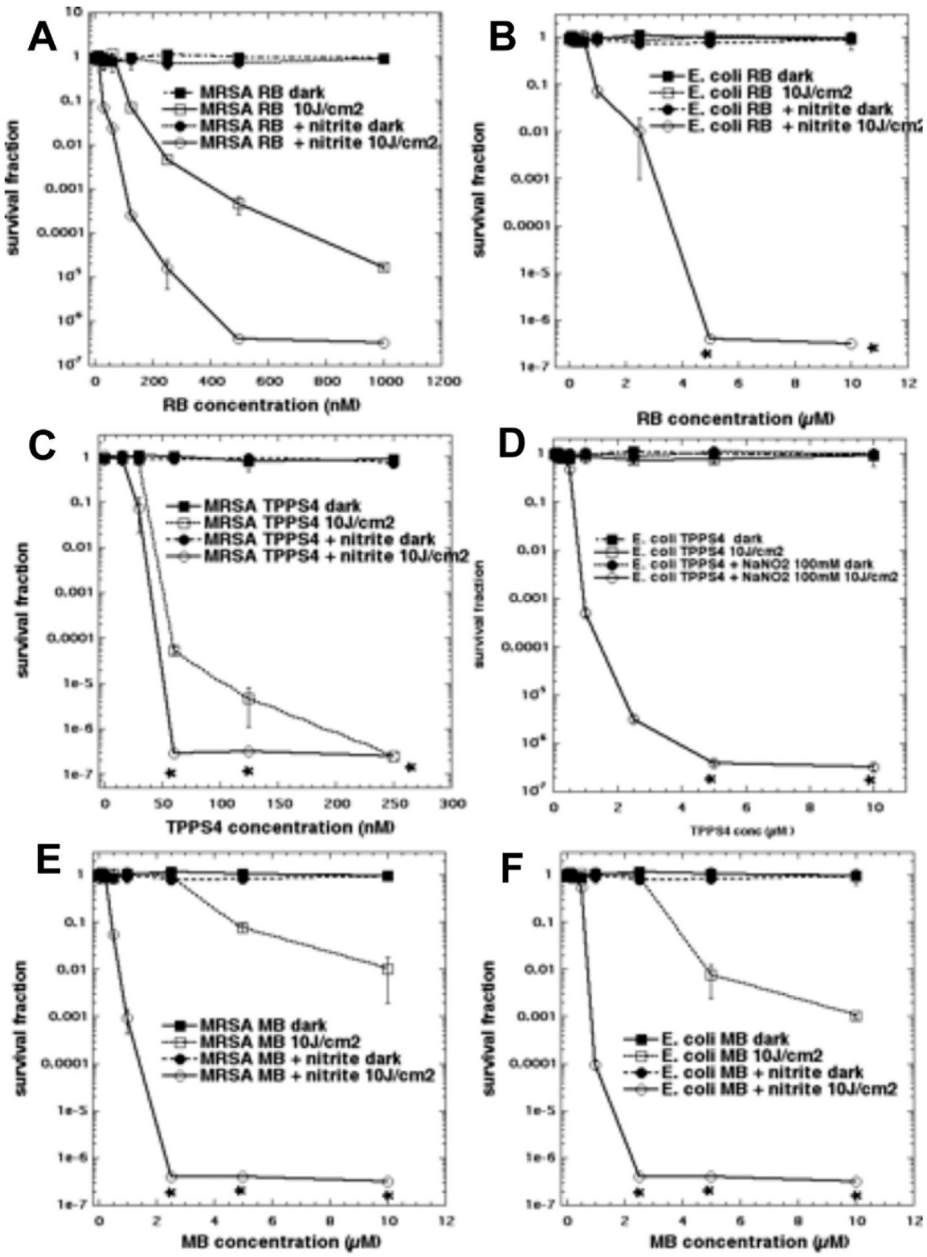

Figure 2. Potentiation of aPDI by addition of sodium nitrite.

Cells were illuminated in solutions with increasing concentrations of PS depending on the type of cells, mixed or not with 100 mM $NaNO_2$ and illuminated with 10 J/cm2 of the appropriate light. (A) MRSA using up to 1 μM RB; (B) *E. coli* using up to 10 μM RB both illuminated (or not) with 10 J/cm 2 540 nm light. (C) MRSA using up to 0.25 μM TPPS4; (D) *E. coli* using up to 10 μM TPPS4 both illuminated (or not) with 10 J/cm^2 415 nm light. (E) MRSA, (F) *E. coli* both using up to 10 μM MB and both illuminated (or not) with 10 J/cm^2 660 nm light.

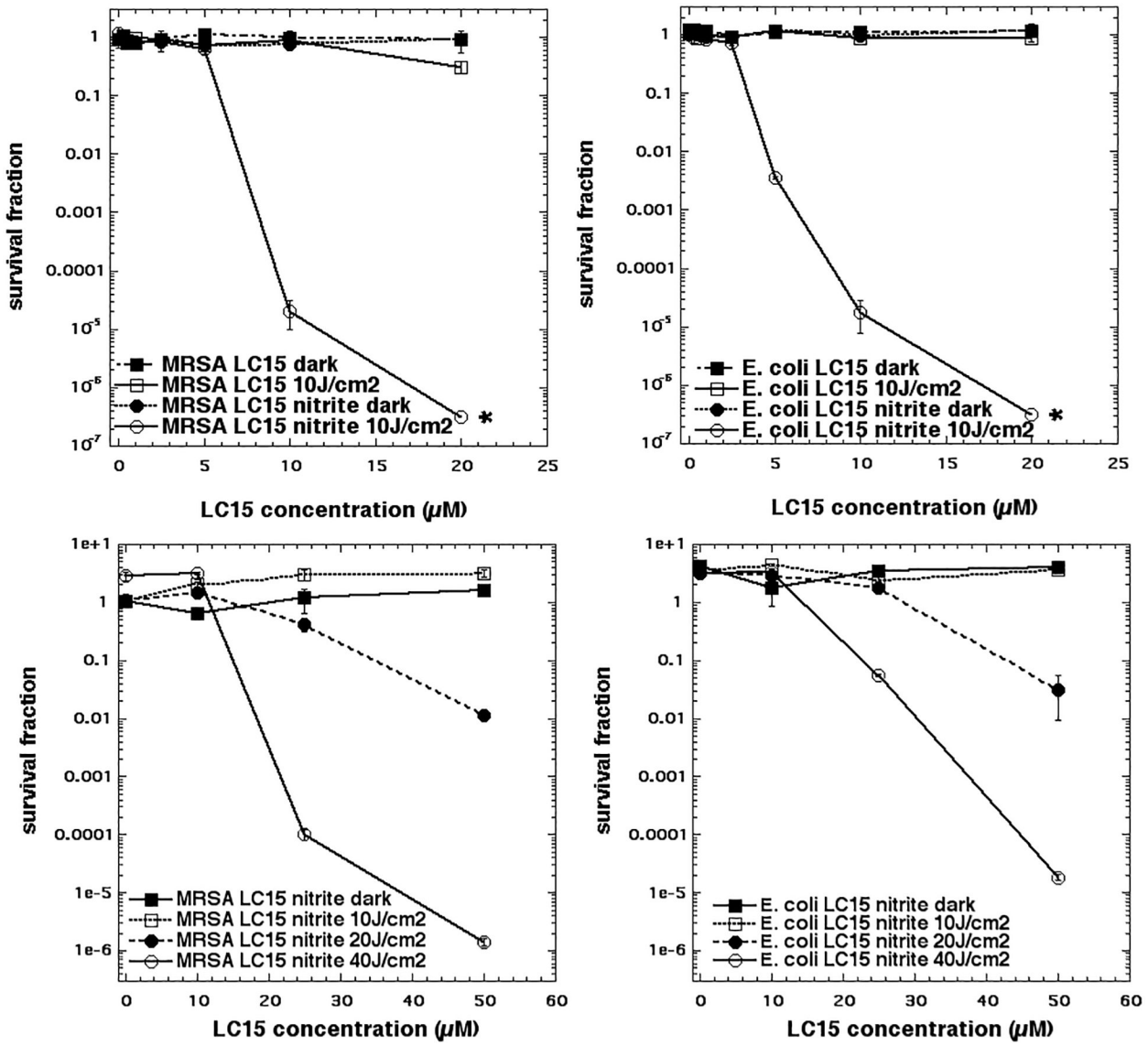

Figure 3. Potentiation of aPDI mediated by LC15 (a decacationic functionalized fullerene) by addition of sodium nitrite.

(A) MRSA and (B) *E. coli* aPDI killing using "in format" with increasing LC15 concentration, and either a fluence of 10 J/cm^2 of 415 nm light or dark, and with or without addition of 100 mM $NaNO_2$. (C) MRSA and (D) *E. coli* aPDI using "after format" where cells were added immediately after light to a mixture of increasing concentrations of LC15 mixed with 200 mM NaNO2, that had been illuminated with 0, 10, 20, or 40 J/cm2 of 415 nm light.

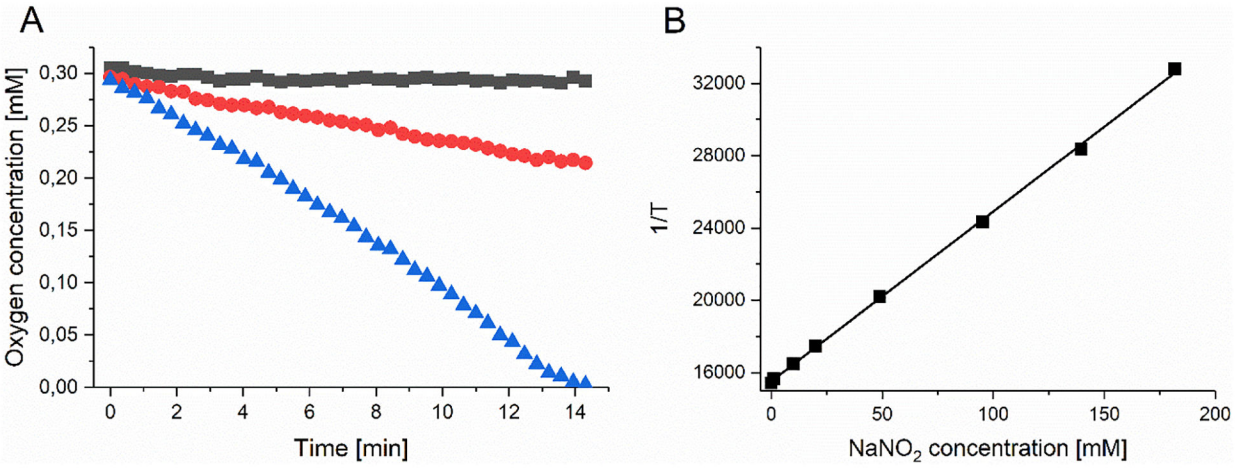

Figure 4. Oxygen consumption and singlet oxygen quenching by nitrite in presence of RB excited by green light.

(A) Oxygen consumption by 5 μM RB excited by green light (35 mW/cm^2) in phosphate buffer (pH 7.0), in the absence (black squares) and presence of 100 mM $NaNO_2$ (red circles) or 200 mM $NaNO_2$ (blue triangles). B) Reciprocal of the determined life time of singlet oxygen as a function of $NaNO_2$ concentration.

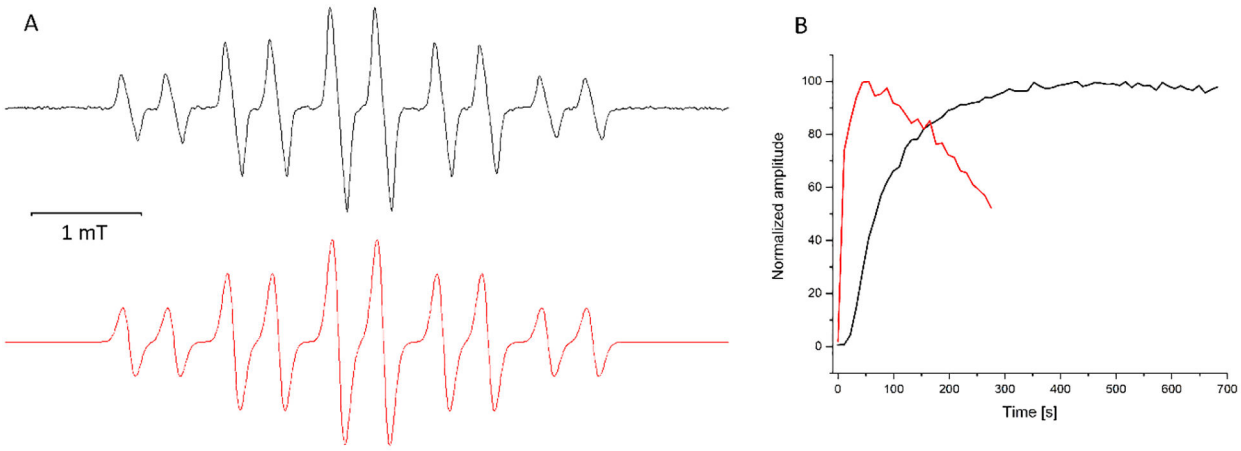

Figure 5. Spin-trapping of nitrogen dioxide.

(A) Experimental (black) and simulated (red) EPR spectra of the spin adduct formed by addition of nitrogen dioxide to aci anion of nitromethane. The experimental EPR spectrum was obtained by rose Bengal (0.02 mM) photosensitzed oxidation of 100 mM nitrate in the presence of 100 mM nitromethane in aqueous solution at pH ~13.5. (B) The photosensitized formation of the spin adduct (as in A) in the absence of oxygen (red trace) and presence of oxgen (black trace).

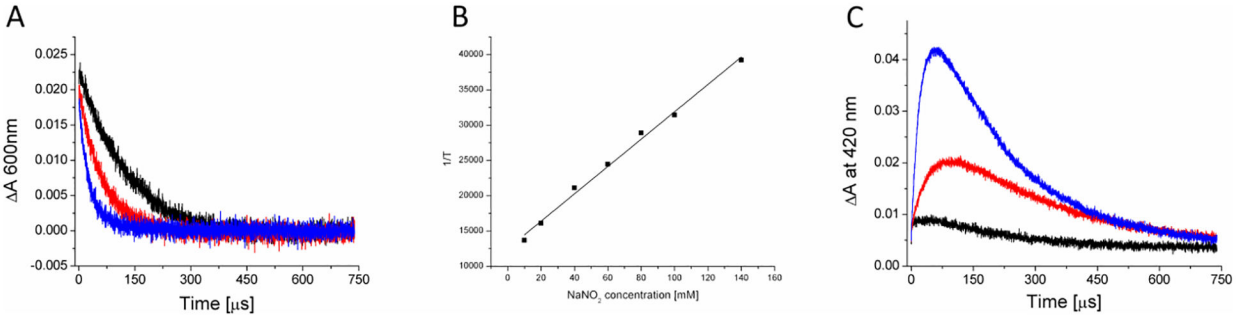

Figure 6. Quenching of RB triplet state by nitrite.

(A) Absorption changes RB triplet excited state monitored at 600 nm (A) or RB anion radical monitored at 420 nm (C) in argon-saturated solution of 0.005 mM Rose Bengal (black trace), and in the presence of 20 mM $NaNO_2$ (red trace) or 100 mM $NaNO_2$ (blue trace). Quenching of RB triplet excited state by $NaNO_2$ (B); the reciprocal of the triplet state lifetime is plotted as a function of $NaNO_2$ concentration.

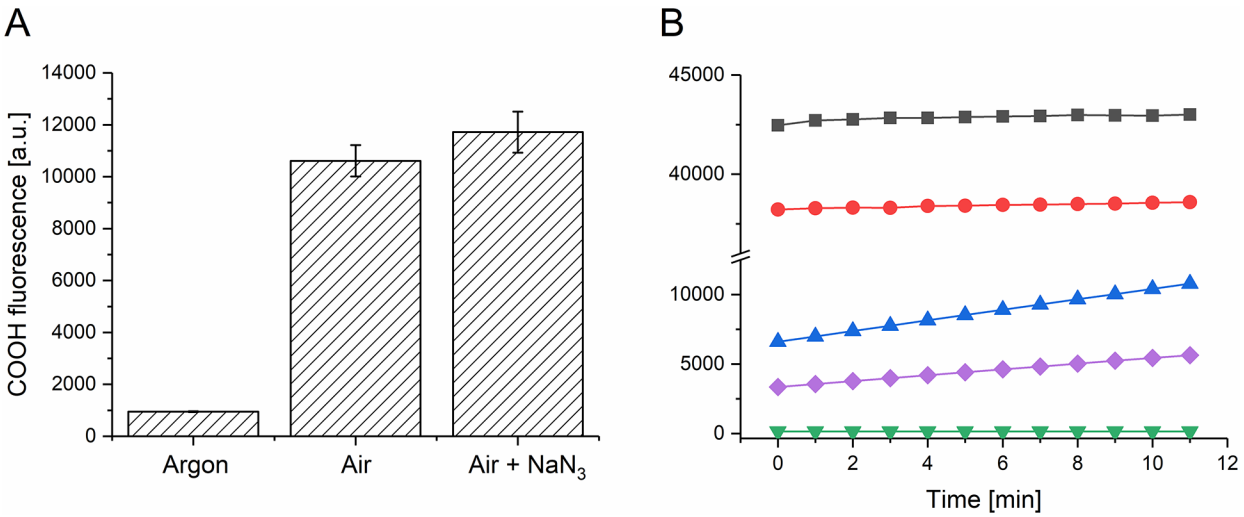

Figure 7. Oxidation of coumarin boronic acid by hydrogen peroxide or RB-mediated photosensitized reaction; effect of nitrite, azide and catalase.

(A) Effect of oxygen and 5mM azide on fluorescence intensity of 7-hydroxycoumarin (COH), the oxidized product of coumarin boronic acid (CBA), generated by photoexcitation of 0.01mM RB in the presence of 100 mM $NaNO_2$. (B) Effect of catalase (250 u) and $NaNO_2$ on hydrogen peroxide induced (three lower curves) or RB photosensitized oxidation of CBA. Black squares samples containing RB, CBA and $NaNO_2$; red circles: the same with addition of catalase; blue triangles: 0.05 mM H_2O_2, CBA; purple diamonds: 0.05 mM H_2O_2, CBA, 100 mM $NaNO_2$; inverted green triangles: 0.05 mM H_2O_2, CBA with 250 u catalase.

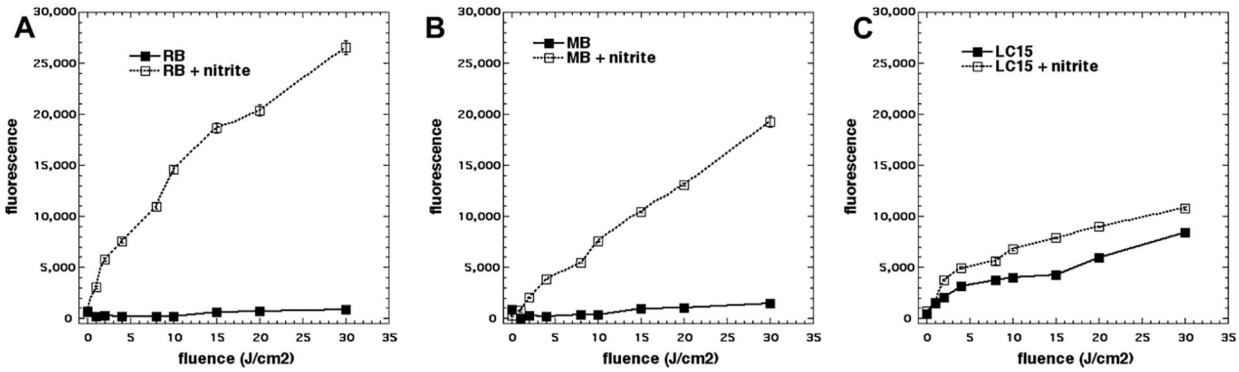

Figure 8. Generation of hydrogen peroxide by illumination of PS in the presence or absence of nitrite (100 mM).

Solutions contained PS (10 μM), $NaNO_2$ (0 or 100 mM) and were illuminated with increasing fluences of (A) RB and 540 nm light; (B) MB and 660 nm light; (C) LC15 and 415 nm light. Aliquots were removed at intervals and added to Amplex Red reagent for fluorescence determination.

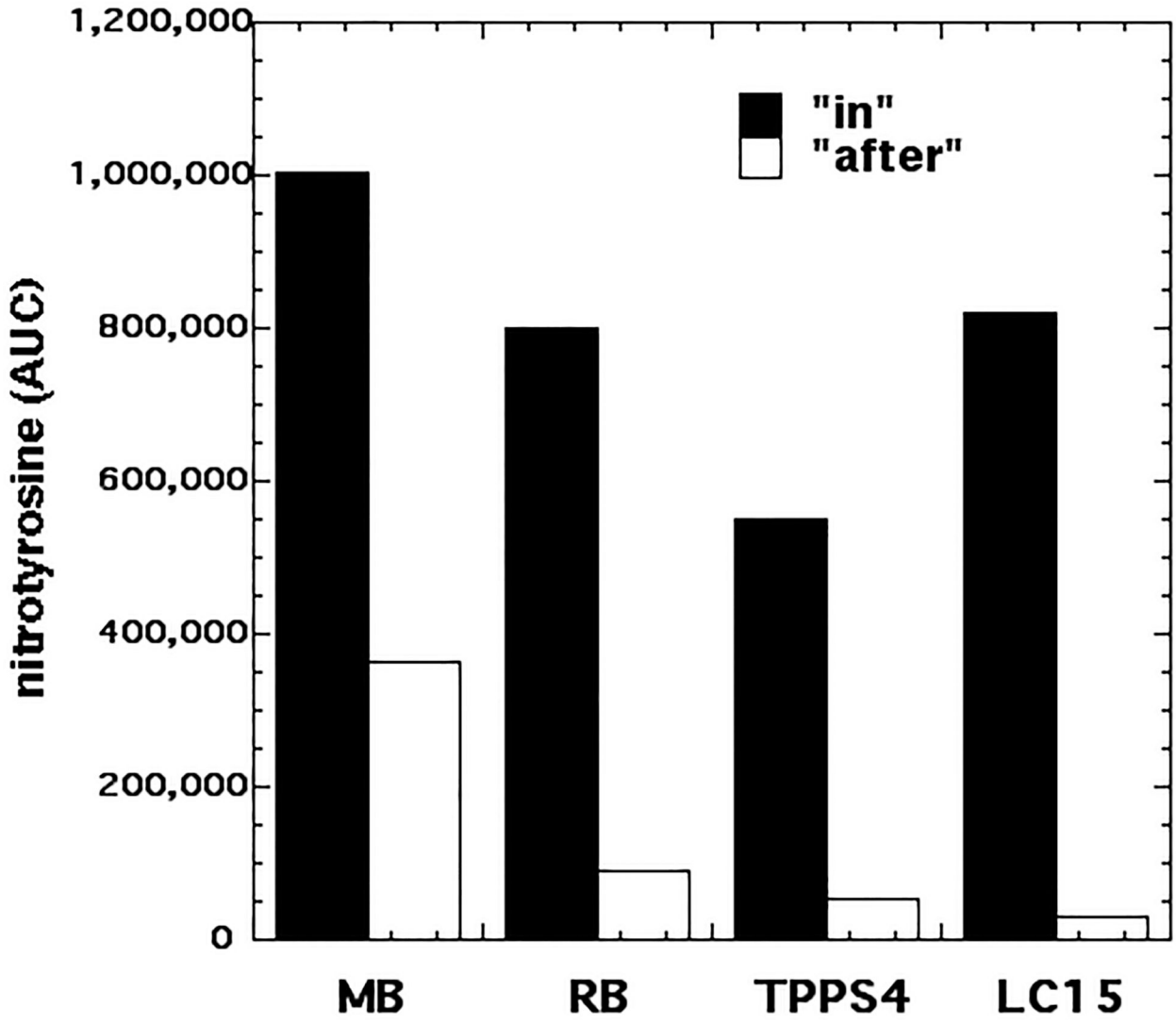

Figure 9. Nitration of tyrosine in solution by PDT using different PS + 100 mM nitrite.

Reactions contained PS (10 μM) plus 100 mM $NaNO_2$ plus 1 mM N-acetyl-tyrosine ethyl ester. The following wavelengths were used MB, 660 nm; RB, 540 nm; TPPS4, 415 nm; LC15, 415 nm and 100 J/cm^2 of each. The “in format” had all components present during light, while for the “after format” the N-acetyl-tyrosine ethyl ester was added after the end of illumination.